Published in final edited form as:
Biomaterials. 2015 February ; 42: 42–51. doi:10.1016/j.biomaterials.2014.11.054.

Minimizing the Non-specific Binding of Nanoparticles to the Brain Enables Active Targeting of Fn14-positive Glioblastoma Cells

Craig S. Schneider[1,2], **Jimena G. Perez**[1,2], **Emily Cheng**[3,4], **Clark Zhang**[5], **Panagiotis Mastorakos**[5], **Justin Hanes**[5], **Jeffrey A. Winkles**[2,3,4], **Graeme F. Woodworth**[1,2,*], and **Anthony J. Kim**[1,2,6,*]

[1]Department of Neurosurgery, University of Maryland School of Medicine, Baltimore, MD 21201 (USA)

[2]Marlene and Stewart Greenebaum Cancer Center, University of Maryland School of Medicine, Baltimore, MD 21201 (USA)

[3]Department of Surgery and Physiology, University of Maryland School of Medicine, Baltimore, MD 21201 (USA)

[4]Center for Vascular and Inflammatory Diseases, University of Maryland School of Medicine, Baltimore, MD 21201 (USA)

[5]Center for Nanomedicine, Johns Hopkins University School of Medicine, 400 North Broadway Street, Baltimore, MD 21231 (USA)

[6]Department of Pharmaceutical Sciences, University of Maryland School of Pharmacy, Baltimore, MD 21201 (USA)

Abstract

A major limitation in the treatment of glioblastoma (GBM), the most common and deadly primary brain cancer, is delivery of therapeutics to invading tumor cells outside of the area that is safe for surgical removal. A promising way to target invading GBM cells is via drug-loaded nanoparticles that bind to fibroblast growth factor-inducible 14 (Fn14), thereby potentially improving efficacy and reducing toxicity. However, achieving broad particle distribution and nanoparticle targeting within the brain remains a significant challenge due to the adhesive extracellular matrix (ECM) and clearance mechanisms in the brain. In this work, we developed Fn14 monoclonal antibody-decorated nanoparticles that can efficiently penetrate brain tissue. We show these Fn14-targeted brain tissue penetrating nanoparticles are able to (i) selectively bind to recombinant Fn14 but not

*Corresponding authors: Graeme F. Woodworth, M.D., Department of Neurosurgery, University of Maryland School of Medicine, 22 South Green Street, Baltimore, MD 21201, gwoodworth@smail.umaryland.edu, Anthony J. Kim, Ph.D., Neurosurgery and Pharmaceutical Sciences, University of Maryland, Baltimore, 655 W. Baltimore Street, Baltimore, MD 21201, akim@smail.umaryland.edu.

brain ECM proteins, (ii) associate with and be internalized by Fn14-positive GBM cells, and (iii) diffuse within brain tissue in a manner similar to non-targeted brain penetrating nanoparticles. In addition, when administered intracranially, Fn14-targeted nanoparticles showed improved tumor cell co-localization in mice bearing human GBM xenografts compared to non-targeted nanoparticles. Minimizing non-specific binding of targeted nanoparticles in the brain may greatly improve the access of particulate delivery systems to remote brain tumor cells and other brain targets.

Keywords

glioblastoma (GBM); brain tissue penetration; surface plasmon resonance (SPR); multiple particle tracking (MPT); extracellular matrix (ECM); targeted nanoparticles; fibroblast growth factor-inducible 14 (Fn14)

Introduction

Glioblastoma (GBM) is the most common form of primary brain cancer and takes more than 15,000 lives in the USA each year, often with devastating neurological consequences [1]. GBM is not curable with surgery alone because tumor cells invade the surrounding brain, rendering complete resection unsafe. Current adjuvant therapies, established by Stupp and colleagues in 2005, use fractionated external beam radiation combined with the orally delivered chemotherapeutic agent Temodar (active drug temozolomide) [2]. Despite these treatments, median survival is still less than 18 months; a major limitation is believed to be delivery of therapeutics to invasive cancer cells, often found many centimeters away from the main tumor mass within functioning brain tissue. Novel treatment approaches such as Gliadel, a biodegradable chemo-loaded polymer wafer that is implanted in the brain after tumor resection, only provides a modest improvement in median survival time due in part to limited drug penetration into the surrounding brain tissue [3–4].

The location of invasive tumor cells presents several barriers to therapeutic delivery. The blood-brain barrier (BBB) regulates the trafficking of molecules to and from the brain. While high grade brain tumors contain some ‘leaky’ neovasculature [5], unresectable tumor cells are consistently found in brain regions with relatively healthy blood vessels. Therapeutics can potentially be delivered to the brain by receptor-mediated transport across the BBB [6–7], mechanical disruption of the BBB via focused ultrasound [8–9], or using hyperosmotic agents [10]; however, it is not yet clear whether sufficient therapeutic doses can be safely achieved. Local delivery approaches, such as Gliadel wafer or convection-enhanced delivery (CED), avoid the complexities associated with the BBB, delivering therapies more directly and deeper into brain tissue [11]. The safety and feasibility of these approaches in human clinical studies has been repeatedly shown [12–13], yet penetration of substances is often still limited [14]. This is largely due to the anisotropic and electrostatically charged extracellular space (ECS) found between brain cells, comprising 15–20% of total brain volume, which acts as a ‘brain penetration barrier’ (BPB) [15–16]. The surrounding extracellular matrix (ECM) and brain cells act as sinks for small molecule drugs, proteins, viral particles, and standard nanoparticles [17–19], thereby limiting their

diffusion and distribution throughout the brain and effective therapeutic results. In addition, perivascular channels serve as critical and efficient brain clearance mechanisms for small molecules and particulate delivery systems, further limiting the distribution, residence time, and efficacy of therapeutic agents [20]. Nanoparticles up to 114 nm in diameter were shown capable of penetrating normal brain tissue, but only if they were exceptionally well-coated with low molecular weight polyethylene glycol (PEG), a hydrophilic and neutrally charged polymer [21]. These characteristics minimize the non-specific, off-target binding of particles to the ECM, thereby enabling improved distribution within brain tissue.

Targeted therapeutics offer the potential for delivering therapies directly to invasive brain cancer cells to improve the desired treatment effects while minimizing unwanted toxicity [22]. Previous studies exploring this approach for invasive brain cancer have included targeting tumor cell surface molecules, such as epidermal growth factor receptor (EGFR) [23], transferrin receptor [24], interleukin-13 (IL-13) and interleukin-4 (IL-4) receptors [13, 25], and tumor-associated ECM components, such as Tenascin C [26]. However, most targeted therapeutic formulations have yet to show improvements in disease progression or survival. Possible issues contributing to this include: (i) adhesive interactions with non-target structures, (ii) target(s) present on only a relatively small percentage of tumor cells or regions, (iii) target(s) not specific for invading cancer cells [14, 27], and (iv) target(s) changes in the context of treatment(s) and/or disease progression [28]. Fibroblast growth factor-inducible 14 (Fn14) is a member of the tumor necrosis factor receptor (TNFR) superfamily and is an emerging molecular target for GBM and other cancers [29–30]. Importantly, Fn14 is minimally expressed in normal human brain but highly expressed in high-grade gliomas with more malignant and invasive characteristics [31]. Elevated Fn14 mRNA and protein expression has been detected in the invasive rim of GBM [31–32], providing the opportunity to target these cells with Fn14-directed therapeutics.

In this study, we explore the tumor-specific targeting capabilities of nanoparticles through a balance of minimized non-specific binding and highly specific binding to invasive brain tumor cells. Based on previous development of particles that efficiently penetrate brain and other physiologic barriers [21, 33–35], we formulated a nanoparticle platform with a dense, low molecular weight PEG surface coating coupled with the ITEM4 monoclonal antibody (mAb) that recognizes the cell surface receptor Fn14 [36]. We thoroughly characterized the (i) specificity of nanoparticle binding to Fn14 and (ii) nonspecific binding to brain ECM components using surface plasmon resonance (SPR) and multiple particle tracking (MPT) assays. *In vitro* and *in vivo* testing was then performed to assess nanoparticle cellular uptake, brain distribution, and tumor cell-specific targeting following direct intracranial injection.

Materials and Methods

Materials

5 kDa MW PEG, methoxy-PEG5k-amine and thiol reactive malemide-PEG5k-amine, were purchased from Creative PEGWorks (Winston Salem, NC). Lab-Tek glass-bottom tissue culture plates and Zeba Spin Columns (7 kDa MW cut-off) were purchased from ThermoFisher Scientific (Rochester, NY). ITEM4 monoclonal antibody was purchased from eBioscience (San Diego, CA). Red (0.1 μm, 540/590 excitation/emission) and Blue (0.1 μm,

350/440 excitation/emission) carboxylate-modified FluoSpheres and Hoechst 34580 were purchased from Invitrogen (Carlsbad, CA). Non-fluorescent carboxyl microspheres (0.1 μm) were purchased from Bang's Laboratories (Fishers, IN). D-Luciferin was obtained from Promega (Madison, WI). Thiol Quantification Assay Kit (Fluorometric) was from Abcam (Cambridge, MA). 1-Ethyl-3-[3-dimethylaminopropyl]carbodiimide hydrochloride (EDC), N-hydroxysulfosuccinimide (sulfo-NHS), Phosphate Buffer, 2-iminothilane hydrochloride, and all other chemicals were purchased from Sigma-Aldrich (St. Louis, MO).

Preparation of ITEM4-SH

ITEM4 was thiol-modified via reaction of free amines with 2-iminothiolane. Briefly, ITEM4 (0.5 mg/mL) was mixed with 2-iminothiolane (400x molar excess to ITEM4) in 100 mM phosphate buffer with EDTA (pH 7.2, 150 mM NaCl, 5 mM EDTA) in a siliconized tube. The reaction was allowed to proceed for 2 h at room temperature to yield thiolated ITEM4 (ITEM4-SH). After the reaction, resulting solution was purified with Zeba Spin Columns (7 kDa MW cut-off) and frozen immediately to avoid potential disulfide bond formation (S-S) between newly generated thiol groups. The degree of thiolation of ITEM4-SH was determined using the Thiol Quantification Assay Kit (Fluorometric assay, Abcam, Cambridge, MA) as per the manufacturer's recommendations. Gluathione (GSH) standard was used to generate a standard curve to determine the number of thiol groups per ITEM4.

Nanoparticle preparation

To formulate brain tissue penetrating 'coated nanoparticles' (CNPs), 100 nm carboxylate-modified polystyrene (PS-COOH) nanoparticles were covalently modified with methoxy-PEG5k-amine by EDC carbodiimide chemistry, following a modified protocol described previously [21, 37]. For protein quantification assay, CNPs were made with 100 nm non-fluorescent PS-COOH nanoparticles. For all other experiments, 100 nm red or blue fluorescent PS-COOH 'uncoated nanoparticles' (UNP) were used. Briefly, PS-COOH nanoparticles (1 mg) were mixed with methoxy-PEG5k-amine (10x equivalent to total COOH groups on surface of PS-COOH particles) in 100 mM phosphate buffer (pH 7.2, 150 mM NaCl), followed by addition of excess sulfo-NHS (~5–6 mg), and EDC (~3–4 mg) to a volume of 500 μL. Particle suspensions were placed on a rotary incubator and the reaction was allowed to proceed for 4 h at 25°C. After the reaction, particles were purified by ultracentrifugation (Amicon Ultra-15 mL 100 kDa MW cut-off) with ultrapure water (3 washes total). CNPs were resuspended in ultrapure water and stored at 4°C until use.

For CNP-ITEM4 nanoparticles, a different proportion of PEG (methoxy-PEG5k-amine to malemide-PEG5k-amine) was used for initial particle PEGylation; specifically, 10 mol % and 50 mol % of maleimide-PEG5k-amine was used for CNP-ITEM4 (low) and CNP-ITEM4 (high) nanoparticles, respectively. ITEM4-SH was conjugated onto the surface of the nanoparticles containing maleimide-functionalized PEG by maleimide-thiol chemistry. Briefly, purified CNP-maleimide particles were mixed with ITEM4-SH (1.2X excess ITEM4-SH to maleimide) in 100 mM phosphate buffer (pH 7.2, 150 mM NaCl) and allowed to react overnight at 4°C. This reaction was performed immediately following nanoparticle PEGylation, as longer incubation times resulted in increased hydrolysis of the maleimide groups. After the reaction, nanoparticles were purified from unconjugated free ITEM4-SH

via dialysis (1000 kDa Float-a-Lyzer dialysis cassettes) against 1X PBS for 5 days. The amount of ITEM4 molecules conjugated on CNP-ITEM4 nanoparticles was quantified via the LavaPep protein assay (Gel Company, San Francisco, CA) using ITEM4 as a standard. Nanoparticle samples were diluted to a concentration of ~100 ug/mL and assayed as per manufacturer's protocol.

Physicochemical characterization of nanoparticles

The physicochemical characteristics of nanoparticles were measured in 15x diluted PBS (~10 mM NaCl, pH 7.4) at 25°C. Hydrodynamic diameter and ζ-potential (surface charge) were determined by dynamic light scattering and laser Doppler anemometry, respectively, using a Zetasizer NanoZS (Malvern Instruments, Southborough, MA). Particle size measurement was performed at 25°C at a scattering angle of 173° and is reported as the number-average mean. The zeta-potential values were calculated using the Smoluchowski equation and is reported as the mean zeta-potential.

Nanoparticle binding to Fn14 extracellular domain

Nanoparticle binding affinities to Fn14 extracellular domain was evaluated by SPR using a Biacore 3000 instrument at 25°C. The Fn14 extracellular domain (Cell Sciences, Canton, MA) was conjugated to a CM5 Biacore chip, with three different Fn14 ligand RU values ranging from 50 to 300. The first flow path (Fc1) was activated and blocked with ethanolamine to serve as a reference for each binding run, as suggested per manufacturer's protocol. The running buffer was degassed 10 mM HEPES buffer (pH 7.4) containing 150 mM NaCl, 0.05% surfactant P-20 with 50 μM EDTA (HBS-P+). For SPR experiments, samples were run at a flow rate of 20 μL/min with an injection time of 3 min followed by a 2.5 min wait time for dissociation, before chip regeneration with either 100 mM phosphoric acid, pH 3 or 10 mM glycine, pH 1.75 (GE Healthcare). IgG isotype (25 nM) was used as a negative control and ITEM4 (25 nM) as a positive control. Nanoparticle binding was assayed with particle concentrations ranging between 1 μg/mL and 200 μg/mL diluted in running buffer. Data were analyzed using Biacore 3000 Evaluation Software, where data from Fc1 was subtracted from the Fc2, Fc3, and Fc4 data to give the final sensorgrams. Equilibrium binding affinities (K_D) were calculated as previously described [38].

Nanoparticle binding to brain extracellular matrix proteins

Brain extracellular matrix (ECM) proteins were isolated from freshly collected mouse brain as previously described [39]. Briefly, resected whole mouse brain was frozen for at least 24 h at −80°C and subsequently thawed and decellularized in a series of steps: ultrapure water (16 h at 4°C), 0.02% trypsin/0.05% EDTA (1 h at 37°C), 3% Triton-X 100 (1 h), 1.0 M sucrose (15 min), ultrapure water (15 min), 4% deoxycholate (1 h), 0.1% periacetic acid in 4% ethanol (2 h), 1X PBS (15 min), ultrapure water (15 min), and 1X PBS (15 min). The decellularized proteins were filtered (0.2 μm filter) to remove insoluble proteins and then frozen and stored at −80°C until use.

The isolated mouse brain ECM proteins were conjugated to the second flow channel (Fc2) of a CM5 Biacore chip with ligand RU values ranging from 140 to 250. The first flow path was activated and blocked with ethanolamine to serve as a reference for each binding run.

For binding experiments, samples were assayed at a flow rate of 20 μL/min with an injection time of 3 min followed by a 2.5 min wait time for dissociation, before chip regeneration with either 100 mM phosphoric acid, pH 3 or 10 mM glycine, pH 1.75 (GE Healthcare). Nanoparticle binding was assayed with particle concentrations ranging between 1 μg/mL and 200 μg/mL, diluted in running buffer.

Cell culture

Human U87 glioblastoma cells that constitutively express firefly luciferase (U87-Luc) were provided by Dr. Andrew Kung (Columbia University Medical Center). In order to generate a GFP-positive U87-Luc cell line, pGIPZ lentiviral particles encoding TurboGFP (provided by Dr. Nhan Tran, TGen) were mixed with 8 μg/mL polybrene and added to subconfluent cultures of U87-Luc cells. Positively transduced cells were enriched by mass sorting the GFP-positive cells using a MoFlo flow cytometer (Dako, Carpinteria, CA). U87-Luc/GFP cells were cultured at 37°C and 5% CO_2 in DMEM (Invitrogen Corp., Carlsbad, CA) supplemented with 10% fetal bovine serum (FBS, Invitrogen Corp.), 0.5 mg/mL G418, and 1% penicillin/streptomycin (Invitrogen Corp.). A mouse embryonic fibroblast (MEF) cell line generated from Fn14-null mice (MEF 3.5−/−) and a derivative stably transfected MEF 3.5−/− cell line expressing human Fn14 (MEF Fn14-V5) [40] were provided by Dr. Matthew Hayden (Columbia University Medical Center). Both cell lines were maintained at 37°C and 5% CO_2 in DMEM supplemented with 10% FBS and 1% penicillin/streptomycin; the Fn14-V5 cell media also contained 10 ug/ml blasticidin.

Evaluation of Fn14 expression in cells

To examine Fn14 surface expression in the U87-Luc/GFP cell line, we performed flow cytometry analysis. Briefly, cells (~10^6) were incubated with no antibody, IgG isotype, or ITEM4 for 30 min on ice. Next, cells were washed 3 times with FACS buffer and a fluorescent secondary antibody (anti-mouse IgG-APC) was added and allowed to incubate for 15 min. After washing 3 times in FACS buffer, cells were assayed for APC mean fluorescence intensity using a FACSCalibur flow cytometer (Becton Dickinson, Franklin Lake, NJ). Data from 10,000 events were gated using forward and side scatter parameters to exclude dying cells and debris.

Fn14 expression in the two MEF cell lines, MEF 3.5 −/− and MEF Fn14-V5, was determined using both Western blot and flow cytometry analyses. For Western blotting, cells were harvested by scraping and lysed in 20 mM HEPES, 150 mM NaCl, 1.5 mM $MgCl_2$, 10% glycerol, and 1% Triton X-100 supplemented with a protease inhibitor cocktail (Sigma-Aldrich, St. Louis, MO) and two phosphatase inhibitor cocktails (Calbiochem, Billerica, MA). The protein concentration of each lysate was determined by BCA protein assay (Pierce Protein Biology, Rockford, IL). Equal amounts of protein were subjected to SDS-PAGE (Life Technologies, Grand Island, NY) and electrotransferred to PVDF membranes (Millipore, Billerica, MA). Membranes were blocked in 5% non-fat dry milk (NFDM) in TBST buffer and then sequentially incubated with either an anti-Fn14 antibody (Cell Signaling Technology, Danvers, MA) or an anti-tubulin antibody (Sigma-Aldrich, St. Louis, MO) and then horseradish peroxidase (HRP)-conjugated secondary antibody (Cell Signaling Technology, Danvers, MA). The membranes were washed in TBST and then

immunoreactive proteins were detected using the Amersham Enhanced Chemiluminescence Plus kit (GE Healthcare, Piscataway, NJ) according to the manufacturer's instructions. For flow cytometry, MEFs (~10^6) were incubated with Mouse Fc Bloc (BD Biosciences, San Jose, CA) for 15 min and then incubated with: no antibody, IgG isotype-APC, or ITEM4-APC for 30 min on ice. Cells were then washed 3 times with FACS buffer and then assayed for APC mean fluorescence intensity by flow cytometry as described above.

Nanoparticle uptake in Fn14-positive and Fn14-negative cells

Nanoparticle uptake in the MEF 3.5−/−, MEF Fn14-V5, and U87-Luc/GFP cell lines was determined via flow cytometry. Briefly, cells were plated in 24-well plates at a seeding density of 10^5 cells per well. Cells were allowed to attach overnight and the following day the media was replaced with serum-free DMEM along with nanoparticles (2 μg per well). Cells were incubated with nanoparticles for 1 h, washed 3 times with 1X PBS, detached with trypsin, and diluted in cold 1X PBS for flow cytometry analysis. Mean fluorescence intensity was analyzed using a BD LSRFortessa flow cytometer (Becton Dickinson, Franklin Lake, NJ). Data from 10,000 events were gated using forward and side scatter parameters to exclude dying cells and debris.

Nanoparticle internalization in Fn14-positive GBM cells

The internalization of CNP-ITEM4 in U87-Luc/GFP cells was confirmed by live-cell confocal microscopy at 37°C and 5% CO_2. Briefly, cells were seeded between 2.0 to 2.5 × 10^3 cells per plate onto Lab-Tek glass-bottom culture plates and incubated overnight at 37°C. After overnight incubation, culture medium was replaced with fresh media before nanoparticles (2 μg per well) were added. Prior to imaging, the U87-Luc/GFP cells were treated for 15 min with Hoechst 34580 (5 μg/ml) to stain the nucleus. Following incubation, cells were washed 3 times with 1X PBS and replaced with Opti-MEM (Invitrogen Corp., Carlsbad, CA). Cells and nanoparticles were then imaged under a Zeiss LSM510 Meta confocal microscope (Carl Zeiss Inc., Thornwood, NY) using a 63X Plan-Apo/1.4 NA oil-immersion lens. For multi-color microscopy, samples were excited with 405, 488, 543 and 633 nm laser lines, and images were captured by multi-tracking to avoid bleed-through between fluorophores.

Nanoparticle transport in rat brain slices

The diffusion of individual fluorescent nanoparticles in rat brain slices was quantified via multiple particle tracking (MPT) as previously described [21]. Briefly, Sprague-Dawley rats (6–8 weeks) were euthanized, the brain was harvested and incubated in artificial cerebrospinal fluid (aCSF, Tocris Bioscience, Bristol, UK) for 10 min on ice. Brain was sliced into 1.5 mm coronal sections using a Zivic brain matrix slicer (Zivic Instruments, Pittsburgh, PA). Slices were added to custom microscope slide chambers and fluorescent nanoparticles were injected (0.5 μL of 20 μg/mL stocks) into the middle of cortical tissue. Slides were sealed with super glue and allowed to incubate at room temperature for a minimum of 15 min before imaging. The movement of individual nanoparticles in brain slices was imaged, at a frame rate of 15 frames/s for a total of 300 frames (20 s), using an inverted epi-fluorescent microscope (Axiovert D1, Zeiss, Thornwood, NY) with a 100x/1.46 NA oil-immersion objective equipped with an Evolve 512 EMCCD camera (Photometrics,

Tucson, AZ). Movies were analyzed using a custom written MATLAB automated tracking code to extract x, y-coordinates of nanoparticles over time, as previously described [41]. At least three rat brains were imaged per each nanoparticle type with at least 100 particles tracked per sample. The geometric mean of the mean squared displacement (MSD) was calculated per sample and the average of different rodent brains was calculated as a function of time scale [33, 41].

Intracranial implantation of U87-Luc/GFP tumors

All animal procedures were approved by the University of Maryland Institutional Animal Care and Use Committee (IACUC) and the Office of Animal Welfare Assurance (OAWA). Athymic nude mice (age, 6–8 weeks) were purchased from the University of Maryland School of Medicine Veterinary Resources. For the tumor implantation procedure, animals were anesthetized via continuous flow of 2 to 3% isoflurane through a nose cone. Using a stereotactic frame and sterile technique, ~4.0×10^5 U87-Luc/GFP GBM cells were injected at a rate of 1 μL/min over 5 min into the left frontal lobe of the brain through a burr hole; drilled 2 mm lateral to the sagittal suture and 1 mm anterior to the coronal suture at a depth of 3 mm below the dura. Mice were given the analgesic buprenorphine (Buprenex, 0.05 mg/kg, subcutaneously) after the surgery. Animals were observed daily for any signs of deterioration or neurological dysfunction. If the symptoms persisted and resulted in debilitation, animals were euthanized according to protocol.

In vivo bioluminescence imaging

Intracranial U87-Luc/GFP mouse tumors were imaged using a Xenogen IVIS system (Caliper Life Sciences, Hopkinton, MA). Anesthesia was induced in an induction chamber with 2.5% isoflurane in 100% oxygen at a flow rate of 1 L/min and maintained in the IVIS system with a 2.0% mixture at 0.5 L/min. The mice were injected with D-luciferin (150 mg/kg, intraperitoneally; dissolved in PBS) and returned to their home cages. Ten minutes following the D-luciferin injection, anesthesia was induced with isoflurane in an induction chamber. The animal was moved to the IVIS imaging chamber and maintained on 2 to 3% isoflurane. Photons emitted from live mice were acquired as photons/s/cm^2/steradian (p/s/cm^2/cm^2/sr) and analyzed using LivingImage software (PerkinElmer, MA).

Intracranial injection of nanoparticles

At day 7 after the implantation of U87-Luc/GFP tumor cells, bioluminescent signal from the engrafted brain tumors was confirmed in each animal. Once tumor signal was confirmed, the animals were anesthetized as described above and nanoparticles suspended in normal saline were administered sterilely into mouse brain (n=3) through the same burr hole using a stereotactic frame. CNP and CNP-ITEM4 (high) nanoparticles in normal saline were loaded into a sterile 30-gauge Hamilton syringe needle, lowered to a depth of 3.5 mm, and injected slowly: 5 μl (0.1 mg/ml nanoparticles) at a rate of 1 μl/min over 5 min.

Nanoparticle distribution in the brain and intracranial human GBM xenograft

The distribution and co-localization of fluorescent nanoparticles with U87-Luc/GFP tumors in the brain was evaluated by imaging brain cryosections. The animals were euthanized with

an overdose of isoflurane 24 h after the injection of nanoparticles. The euthanized animals were perfused with 30 mL of 1X PBS after which the brains were carefully removed, embedded in Optimal Cutting Temperature (OCT), and stored at −80°C. A cryostat (Leica CM3050 S) was used to cut serial 10 μm sagittal brain sections and mounted on positively charged microscope slides. The brain sections were stained with Prolong Gold antifade with or without DAPI (Invitrogen, Carlsbad, CA), sealed with coverslips, and imaged for cell nuclei (dark blue), CNPs (light blue), GFP-positive U87 tumors (green), and CNP-ITEM4 (high) nanoparticles (red) using a Nikon epifluorescence microscope under 10x and 20x magnification. High resolution stitched images (6 × 6) were obtained by using the montage imaging feature in the Nikon NX 2 software. Microscope settings were carefully optimized to avoid background fluorescence based on non-injected control mouse brains, where the exposure time for each channels were kept constant throughout the study.

Statistical analysis

Statistical analysis of data was performed by a two-tailed Student's t test assuming unequal variances or one-way analysis of variance (ANOVA) followed by Tukey HSD or Games-Howell tests using SPSS 18.0 software (SPSS Inc., Chicago, IL). Differences were considered to be statistically significant at a level of $P < 0.05$.

Results

Synthesis and characterization of Fn14-targeted Nanoparticles

We synthesized a variety of polystyrene (PS)-based brain tissue penetrating 'coated nanoparticles' (CNPs) that were surface-functionalized with a well-characterized antibody, ITEM4, that binds strongly to Fn14. Reaction conditions, including the molar excess of 2-iminothiolane to ITEM4 and the ratio of malemide-PEG5k-amine to methoxy-PEG5k-amine, were optimized to produce CNPs with different surface densities of ITEM4 (Figure S1). We synthesized three sets of PEG-coated nanoparticles: no ITEM4 (CNP), decorated with a low density of ITEM4 (CNP-ITEM4 (low)), or decorated with a high density of ITEM4 (CNP-ITEM4 (high)) and compared these formulations with conventional, uncoated nanoparticles (UNP) (Table 1). CNP, CNP-ITEM4 (low) and CNP-ITEM4 (high) exhibited larger hydrodynamic diameters and more near neutral ζ-potential compared to UNP, as expected for nanoparticles with dense PEG coatings. CNP-ITEM4 (low), and CNP-ITEM4 (high) displayed a slightly more negative surface charge compared to CNP. We quantified the number of ITEM4 molecules on the surface of nanoparticles and determined there were ~11 and ~56 ITEM4 molecules per particle for CNP-ITEM4 (low) and CNP-ITEM4 (high) nanoparticles, respectively.

Biacore screening of nanoparticles for Fn14 binding

To test the ability of CNP-ITEM4 nanoparticles to bind Fn14, the Fn14 extracellular domain was functionalized to the surface of a Biacore chip and we measured the binding of ITEM4 (unmodified), ITEM4-SH (thiol-modified for surface conjugation to nanoparticles), and CNP formulations with different surface densities of ITEM4. ITEM4 and ITEM4-SH bound similarly, indicating that thiol-modification of ITEM4 does not significantly affect the binding activity of ITEM4 to Fn14 (Figure 1A). CNP exhibited no appreciable Fn14

binding, whereas both CNP-ITEM4 (low) and CNP-ITEM4 (high) displayed significant Fn14 binding on the chip (Figure 1B). In addition, the binding of CNP-ITEM4 nanoparticles to the chip was proportional to the surface density of ITEM4, as CNP-ITEM4 (high) exhibited stronger binding compared to CNP-ITEM4 (low). To confirm the specificity of CNP-ITEM4 binding to the Fn14 Biacore chip, we first blocked available Fn14 binding sites with excess ITEM4 (500 nM), after which CNP-ITEM4 (high) particles were allowed to bind to the chip. We found that CNP-ITEM4 (high) bound to the Fn14 Biacore chip that was pretreated with control IgG, but not to the chip treated with excess ITEM4 (Figure S2). To quantify the binding of various CNP-ITEM4 formulations to the Fn14 extracellular domain, we determined their binding affinities (K_D) by measuring the binding at various concentrations. The binding data and appropriate fitting procedures for ITEM4 and ITEM4-SH are provided in Figure S3. The measured K_D for CNP-ITEM4 (low) and CNP-ITEM4 (high) were 106 pM and 24 pM, respectively (Figure S4); they were ~15- and ~65-fold higher than the binding affinity of ITEM4 alone. Tabulated K_D values for the various ITEM4 and CNP formulations are provided in Table 2.

Biacore screening of nanoparticles for non-specific binding to brain ECM proteins

To screen nanoparticles for non-specific binding to brain ECM, we functionalized mouse brain ECM components to the surface of a Biacore chip and evaluated the binding of various nanoparticle formulations. As a positive control, we measured the non-specific binding of uncoated nanoparticles (UNP), as these particles have been shown previously to be nearly completely immobilized when delivered into the rodent brain [21]. UNP bound strongly to the surface of the ECM Biacore chip (Figure 2), and these particles did not appreciably desorb from the chip with standard Biacore regeneration procedures (data not shown). Thus, a freshly prepared ECM Biacore chip was used for the remainder of the experiments. None of the CNP formulations that we studied (CNP, CNP-ITEM4 (low) and CNP-ITEM4 (high)) bound appreciably to the ECM chip, suggesting minimal non-specific interactions between the nanoparticles and the brain ECM proteins (Figure 2).

Nanoparticle uptake in Fn14-negative and Fn14-positive cells

To confirm our CNP-ITEM4 nanoparticle binding results from the Biacore assay, we measured the cellular uptake of our CNP formulations via flow cytometry. First, we measured the uptake of CNP-ITEM4 with two mouse embryonic fibroblast (MEF) cell lines: MEF 3.5 −/− and MEF Fn14-V5. The MEF 3.5 −/− cells were generated from Fn14-null mice and therefore do not express Fn14, as assayed by either Western blot analysis (Figure 3A) or flow cytometry (Figure 3B). MEF Fn14-V5 cells were produced via infection of the MEF 3.5 −/− cell line with a lentivirus encoding human Fn14. Fn14 expression in these cells was confirmed by Western blot and flow cytometry assays (Figure 3 A and B). CNP-ITEM4 nanoparticle uptake by the MEF cell lines was determined via flow cytometry. There was no difference in cellular uptake between CNP and CNP-ITEM4 (high) in MEF 3.5−/− cells; in contrast, CNP-ITEM4 (high) uptake was ~2.5-fold greater than CNP uptake when these nanoparticles were added to the MEF Fn14-V5 cells (Figure 3C).

Second, we examined nanoparticle uptake in human U87-Luc/GFP GBM cells. These cells express Fn14, as measured by Western blotting (Figure S5) and flow cytometry (Figure 4A).

We observed a statistically significant increase in CNP uptake in these cells with increasing ITEM4 density (Figure 4B). Specifically, the cellular uptake efficiency of CNP-ITEM4 (low) and CNP-ITEM4 (high) was ~1.25-fold and ~3.5-fold higher, respectively, compared to CNP alone. To test whether the enhanced CNP-ITEM4 uptake was the result of a specific interaction between ITEM4 and Fn14, we performed a competitive inhibition assay with free ITEM4 antibody. Addition of excess free ITEM4 to cells, prior to particle addition, significantly inhibited the uptake of CNP-ITEM4 (high) to the same levels as that observed for non-targeted CNP (Figure 4C). In contrast, no inhibition of CNP-ITEM4 uptake was observed when the same amount of IgG isotype control protein was preincubated with U87-Luc/GFP cells. To confirm that CNP-ITEM4 nanoparticles were internalized within cells and not solely associated with Fn14 on the cell surface, we performed live-cell confocal microscopy imaging (Figure 4D–G). Intracellular localization of CNP-ITEM4 was confirmed via z-stack analysis of cells stained with Hoechst 34580 (Figure 4G).

Nanoparticle transport in brain tissue

MPT was used to test the diffusion rates of individual nanoparticles in *ex vivo* rat brain slices. Representative trajectories of nanoparticles are shown in Figure 5A, from which it is clear that UNP were immobilized in brain tissue. In contrast, all three CNP formulations tested, CNP, CNP-ITEM4 (low) and CNP-ITEM4 (high), exhibited more diffusive Brownian-like trajectories. This can be quantitatively observed by the upward shift in the MSD vs time scale (τ) curve for CNP, CNP-ITEM4 (low) and CNP-ITEM4 (high) compared to UNP (Figure 5B). The calculated MSD at a time scale (τ) = 1 s for CNP formulations were more than an order of magnitude greater than UNP (Figure 5C). The difference in the calculated MSD (at $\tau = 1$) between UNP and all CNP formulations was statistically significant; however, there was no statistical difference between CNP, CNP-ITEM4 (low) and CNP-ITEM4 (high). We also estimated the number of immobilized particles for each of the nanoparticle formulations based on the MPT transport data (Figure S6). The percentage of particles were classified as immobilized if the displayed MSD values at a time scale (τ) of 1 second were less than the MSD for a particle that has moved one particle diameter from it's initial position. Nearly ~90% of UNP were effectively immobilized in brain tissue, whereas only 25% to 45% of CNP were immobile depending on the formulation; however, a statistically significant difference was only observed between UNP and CNP-ITEM4 (high).

Nanoparticle distribution following intracranial administration into human GBM xenografts

To test the performance of Fn14-targeted nanoparticles *in vivo*, we administered fluorescent nanoparticles - CNP and CNP-ITEM4 (high) - to athymic nude mice bearing orthotopic U87-Luc/GFP GBM tumors. Luciferase-expressing U87 tumors were evident in the brain 7 days after tumor implantation (Figure S7). CNP and CNP-ITEM4 (high) nanoparticles were co-injected at the same stereotactic coordinates that were used for the tumor cell implantation. The mice were euthanized at 24 h after nanoparticle injection and brains were isolated. Cryosections were prepared and imaging conducted to assess tissue distribution of the nanoparticles and co-localization with the GFP-expressing brain tumor cells (Figure 6A–D). CNP and CNP-ITEM4 (high) nanoparticles were both distributed uniformly in the brain; however, we found a greater association of CNP-ITEM4 (high) with GFP-expressing tumor

cells compared to untargeted CNP (Figure 6D). These results demonstrate that our CNP-ITEM4 can penetrate within brain tissue and selectively target remote experimental GBM tumors. It is important to note that the distribution of particles represented in Figure 6 may not characterize the eventual location(s) or duration of the particle groups in the brain over time. Additional studies are currently underway to further elucidate these matters.

Discussion

In this study, we extended a previous work describing a formulation strategy that enables relatively free movement of nanoparticles within brain tissue through minimal nonspecific binding and consideration of size-related steric restrictions [21]. This enhanced diffusivity permitted the development of a selective targeting strategy to model particulate drug carriers to experimental xenograft tumors within the brain. When administered intracranially, ~100 nm PEG-coated, Fn14-targeted nanoparticles (CNP-ITEM4) showed broad distribution in the brain and selective targeting to the Fn14-positive tumor cells in mice bearing human U87 tumor xenografts. Tumor cells located at distant sites, deep within the brain, likely contribute to tumor recurrence since they cannot be removed with surgery and are the most difficult to treat due to the close proximity of functioning brain cells and the intact BBB. Therefore, we hypothesized that reducing the non-specific binding towards the brain ECM is a critical rate-limiting step in the development of effective targeted treatments. We show here that tumor specific targeting of nanoparticles can be enhanced through a balance of (i) minimal non-specific binding to provide broad particle dispersion and (ii) selective binding to distant glioma cells via Fn14, a cell surface molecule expressed by these cells.

Fn14, the smallest member of the TNFR superfamily, is an emerging molecular target for GBM therapy [29, 42]. Fn14 is minimally expressed in normal human brain, but highly expressed in malignant gliomas with more aggressive and invasive characteristics [31]. Importantly, elevated Fn14 mRNA and protein expression has been detected in the rim of invading glioma cells with less elevation in the tumor core, which provides the opportunity to target the invasive cells with Fn14-directed therapeutics [30–32]. In this work, we used the Fn14-specific mAb ITEM4 as the targeting moiety for this purpose. This targeting molecule was chosen based on previous studies revealing that Fn14-positive cancer cells are vulnerable to ITEM4-based immunotoxins [43–45]. Although mAbs introduce some inherent limitations; specifically, their relatively large size and the presence of the Fc region may contribute to off-target effects (e.g. cell binding, recognition, and clearance), the highly specific binding of a full mAb enabled an important proof-of-concept determination in this study.

Current therapies and clinical trials using non-targeted and targeted therapeutic strategies for GBM have been affected by limited distribution within the brain. For example, carmustine was shown to diffuse a few millimeters from the implantable Gliadel polymer wafer surface during the majority of the release phase *in vivo* [15]. In addition, recent clinical trials have shown that CED of targeted toxins, such as IL-13-, IL-4-, and transferrin-conjugated toxins, as well as viral particles, failed to show survival improvements. This is most likely because penetration and distribution of the therapeutic agent is still limited [14, 46]. In other examples, Voges *et al*. and Zhou *et al*. showed that even following CED, the ECM acts as a

diffusion barrier limiting the spatial distribution of therapeutic nanoparticles [19, 47–48]. Therefore, the diffusion and distribution of therapeutics within the brain and brain tumors is a major limitation to achieving significant treatment efficacy, even with these local therapeutic approaches. This is thought to be especially important for GBM given the invasive, migratory nature of the disease [18].

Recent studies suggest targeted nanoparticle therapies offer the potential of delivering agents directly to invading tumor cells to improve treatment efficacy while minimizing associated toxicities [22]. In one example, chlorotoxin conjugated chitosan-based nanoparticles showed preferential accumulation in gliomas in mice [49]. In other study, liposomes conjugated with IL-13 were able to deliver doxorubicin specifically to glioma cells [25]. However, achieving broad particle distribution and therapeutically relevant nanoparticle targeting remain a challenge. Nanoparticle diffusion in the brain predominantly takes place through narrow tortuous spaces between cells [15, 50]. The ECM, the main component of the extracellular space, imposes an adhesive and steric barrier to the diffusion of nanoparticles through the brain parenchyma, as shown with the uncoated 100 nm nanoparticles (UNP) in this study. Vargova and colleagues also found that the ECS volume fraction and tortuosity increase with glioma histopathological grade, further increasing the diffusion barriers for small molecules and nanoparticles [16]. Hence, limited penetration of targeted therapeutic nanoparticles in the ECS remains a key hurdle to (i) effective drug distribution within brain tumor-affected regions, and (ii) targeting to tumor-related structures where moving through brain tissue and only attaching to specific structures may improve efficacy and reduce toxicity.

In this study, we focused on minimizing the non-specific binding to the brain ECM in the design of a targeted brain tissue penetrating nanoparticle system, which then permitted selective tumor cell targeting through minimal off-target binding. The demonstration here of enhanced particle distribution and tumor targeting suggests a promising opportunity for the development of new formulation strategies for brain and other cancers. Based on the formulation characteristics developed here in model polystyrene nanoparticles, we envision drug delivery platforms that can be readily translated into new therapeutic systems, such as biodegradable PLGA nanoparticles. A similar strategy can be adapted to a variety of different FDA-approved polymers, drugs, and targeting ligands. These results support further investigation into the use of the Fn14-targeted nanoparticle platform with CED and other novel delivery approaches for GBM to potentially improve the distribution and duration of therapeutic effects. Fn14 is also overexpressed in a broad range of other cancers outside the brain [29–30] including melanoma [43], breast [51], prostate [52], and non-small cell lung cancer [53]. Accordingly, we envision that our Fn14-targeted nanoparticle platform may have broader applicability beyond GBM patient therapy in the future.

Conclusion

In summary, we have developed a nanoparticle platform that can diffuse and penetrate within brain tissue and selectively target remote experimental GBM tumors. We show here that tumor specific targeting of nanoparticles can be achieved through a balance of minimal non-specific binding and specific binding to distant glioma cells. This formulation approach

may improve drug efficacy while limiting many of the side effects and risks of free drug and non-targeted therapies.

Supplementary Material

Refer to Web version on PubMed Central for supplementary material.

Acknowledgements

This work was supported in part by the National Institutes of Health (K12NS080223, K25EB018370, K08NS09043, R01CA164789, and U54CA151838), a Passano Foundation Physician Scientist Award, and a PhRMA Foundation Research Starter Grant in Pharmaceutics. We thank Molly Migliorini, Yinghua Zhang, and Dudley Strickland for their help with the surface plasmon resonance (Biacore) experiments and Colin Brinkman and Mark Williams with the flow cytometry experiments. We also thank Andrew Kung and Matthew Hayden for providing cell lines, Nhan Tran for providing lentiviral particles, and Benjamin Schuster for valuable discussions and technical support with the multiple particle tracking assay. The content is solely the responsibility of the authors and does not necessarily represent the official views of the National Institutes of Health.

References

1. Wen PY, Kesari S. Malignant gliomas in adults. N Engl J Med. 2008; 359:492–507. [PubMed: 18669428]
2. Stupp R, Mason WP, van den Bent MJ, Weller M, Fisher B, Taphoorn MJ, et al. Radiotherapy plus concomitant and adjuvant temozolomide for glioblastoma. N Engl J Med. 2005; 352:987–996. [PubMed: 15758009]
3. Fung LK, Shin M, Tyler B, Brem H, Saltzman WM. Chemotherapeutic drugs released from polymers: distribution of 1,3-bis(2-chloroethyl)-1-nitrosourea in the rat brain. Pharm Res. 1996; 13:671–682. [PubMed: 8860421]
4. Brem H, Piantadosi S, Burger PC, Walker M, Selker R, Vick NA, et al. Placebo-controlled trial of safety and efficacy of intraoperative controlled delivery by biodegradable polymers of chemotherapy for recurrent gliomas. The Polymer-brain Tumor Treatment Group. Lancet. 1995; 345:1008–1012. [PubMed: 7723496]
5. Tate MC, Aghi MK. Biology of angiogenesis and invasion in glioma. Neurotherapeutics. 2009; 6:447–457. [PubMed: 19560735]
6. Jain KK. Nanobiotechnology-based strategies for crossing the blood-brain barrier. Nanomedicine (Lond). 2012; 7:1225–1233. [PubMed: 22931448]
7. Ulbrich K, Hekmatara T, Herbert E, Kreuter J. Transferrin- and transferrin-receptor-antibody-modified nanoparticles enable drug delivery across the blood-brain barrier (BBB). Eur J Pharm Biopharm. 2009; 71:251–256. [PubMed: 18805484]
8. Vykhodtseva N, McDannold N, Hynynen K. Progress and problems in the application of focused ultrasound for blood-brain barrier disruption. Ultrasonics. 2008; 48:279–296. [PubMed: 18511095]
9. Nance E, Timbie K, Miller GW, Song J, Louttit C, Klibanov AL, et al. Non-invasive delivery of stealth, brain-penetrating nanoparticles across the blood-brain barrier using MRI-guided focused ultrasound. J Control Release. 2014; 189:123–132. [PubMed: 24979210]
10. Kroll RA, Neuwelt EA. Outwitting the blood-brain barrier for therapeutic purposes: osmotic opening and other means. Neurosurgery. 1998; 42:1083–1099. discussion 99–100. [PubMed: 9588554]
11. Bobo RH, Laske DW, Akbasak A, Morrison PF, Dedrick RL, Oldfield EH. Convection-enhanced delivery of macromolecules in the brain. Proc Natl Acad Sci U S A. 1994; 91:2076–2080. [PubMed: 8134351]
12. Bruce JN, Fine RL, Canoll P, Yun J, Kennedy BC, Rosenfeld SS, et al. Regression of recurrent malignant gliomas with convection-enhanced delivery of topotecan. Neurosurgery. 2011; 69:1272–1279. discussion 9–80. [PubMed: 21562434]

13. Kunwar S, Chang S, Westphal M, Vogelbaum M, Sampson J, Barnett G, et al. Phase III randomized trial of CED of IL13-PE38QQR vs Gliadel wafers for recurrent glioblastoma. Neuro Oncol. 2010; 12:871–881. [PubMed: 20511192]
14. Sampson JH, Archer G, Pedain C, Wembacher-Schroder E, Westphal M, Kunwar S, et al. Poor drug distribution as a possible explanation for the results of the PRECISE trial. J Neurosurg. 2010; 113:301–309. [PubMed: 20020841]
15. Sykova E, Nicholson C. Diffusion in brain extracellular space. Physiol Rev. 2008; 88:1277–1340. [PubMed: 18923183]
16. Vargova L, Homola A, Zamecnik J, Tichy M, Benes V, Sykova E. Diffusion parameters of the extracellular space in human gliomas. Glia. 2003; 42:77–88. [PubMed: 12594739]
17. Allard E, Passirani C, Benoit JP. Convection-enhanced delivery of nanocarriers for the treatment of brain tumors. Biomaterials. 2009; 30:2302–2318. [PubMed: 19168213]
18. Woodworth GF, Dunn GP, Nance EA, Hanes J, Brem H. Emerging insights into barriers to effective brain tumor therapeutics. Front Oncol. 2014; 4:126. [PubMed: 25101239]
19. Zhou J, Patel TR, Sirianni RW, Strohbehn G, Zheng MQ, Duong N, et al. Highly penetrative, drug-loaded nanocarriers improve treatment of glioblastoma. Proc Natl Acad Sci U S A. 2013; 110:11751–11756. [PubMed: 23818631]
20. Iliff JJ, Wang M, Liao Y, Plogg BA, Peng W, Gundersen GA, et al. A paravascular pathway facilitates CSF flow through the brain parenchyma and the clearance of interstitial solutes, including amyloid beta. Sci Transl Med. 2012; 4:147ra11.
21. Nance EA, Woodworth GF, Sailor KA, Shih TY, Xu Q, Swaminathan G, et al. A dense poly(ethylene glycol) coating improves penetration of large polymeric nanoparticles within brain tissue. Sci Transl Med. 2012; 4:149ra19.
22. Tzeng SY, Green JJ. Therapeutic nanomedicine for brain cancer. Ther Deliv. 2013; 4:687–704. [PubMed: 23738667]
23. Hadjipanayis CG, Machaidze R, Kaluzova M, Wang L, Schuette AJ, Chen H, et al. EGFRvIII antibody-conjugated iron oxide nanoparticles for magnetic resonance imaging-guided convection-enhanced delivery and targeted therapy of glioblastoma. Cancer Res. 2010; 70:6303–6312. [PubMed: 20647323]
24. Pang Z, Gao H, Yu Y, Guo L, Chen J, Pan S, et al. Enhanced intracellular delivery and chemotherapy for glioma rats by transferrin-conjugated biodegradable polymersomes loaded with doxorubicin. Bioconjug Chem. 2011; 22:1171–1180. [PubMed: 21528923]
25. Madhankumar AB, Slagle-Webb B, Mintz A, Sheehan JM, Connor JR. Interleukin-13 receptor-targeted nanovesicles are a potential therapy for glioblastoma multiforme. Mol Cancer Ther. 2006; 5:3162–3169. [PubMed: 17172420]
26. Reardon DA, Akabani G, Coleman RE, Friedman AH, Friedman HS, Herndon JE 2nd, et al. Phase II trial of murine (131)I-labeled antitenascin monoclonal antibody 81C6 administered into surgically created resection cavities of patients with newly diagnosed malignant gliomas. J Clin Oncol. 2002; 20:1389–1397. [PubMed: 11870184]
27. Rich JN, Bigner DD. Development of novel targeted therapies in the treatment of malignant glioma. Nat Rev Drug Discov. 2004; 3:430–446. [PubMed: 15136790]
28. Sampson JH, Heimberger AB, Archer GE, Aldape KD, Friedman AH, Friedman HS, et al. Immunologic escape after prolonged progression-free survival with epidermal growth factor receptor variant III peptide vaccination in patients with newly diagnosed glioblastoma. J Clin Oncol. 2010; 28:4722–4729. [PubMed: 20921459]
29. Winkles JA. The TWEAK-Fn14 cytokine-receptor axis: discovery, biology and therapeutic targeting. Nat Rev Drug Discov. 2008; 7:411–425. [PubMed: 18404150]
30. Cheng E, Armstrong CL, Galisteo R, Winkles JA. TWEAK/Fn14 Axis-Targeted Therapeutics: Moving Basic Science Discoveries to the Clinic. Front Immunol. 2013; 4:473. [PubMed: 24391646]
31. Tran NL, McDonough WS, Savitch BA, Fortin SP, Winkles JA, Symons M, et al. Increased fibroblast growth factor-inducible 14 expression levels promote glioma cell invasion via Rac1 and nuclear factor-kappaB and correlate with poor patient outcome. Cancer Res. 2006; 66:9535–9542. [PubMed: 17018610]

32. Fortin SP, Ennis MJ, Savitch BA, Carpentieri D, McDonough WS, Winkles JA, et al. Tumor necrosis factor-like weak inducer of apoptosis stimulation of glioma cell survival is dependent on Akt2 function. Mol Cancer Res. 2009; 7:1871–1881. [PubMed: 19861406]
33. Kim AJ, Boylan NJ, Suk JS, Hwangbo M, Yu T, Schuster BS, et al. Use of single-site-functionalized PEG dendrons to prepare gene vectors that penetrate human mucus barriers. Angew Chem Int Ed Engl. 2013; 52:3985–3988. [PubMed: 23460577]
34. Ensign LM, Tang BC, Wang YY, Tse TA, Hoen T, Cone R, et al. Mucus-penetrating nanoparticles for vaginal drug delivery protect against herpes simplex virus. Sci Transl Med. 2012; 4:138ra79.
35. Lai SK, O'Hanlon DE, Harrold S, Man ST, Wang YY, Cone R, et al. Rapid transport of large polymeric nanoparticles in fresh undiluted human mucus. Proc Natl Acad Sci U S A. 2007; 104:1482–1487. [PubMed: 17244708]
36. Nakayama M, Ishidoh K, Kojima Y, Harada N, Kominami E, Okumura K, et al. Fibroblast growth factor-inducible 14 mediates multiple pathways of TWEAK-induced cell death. J Immunol. 2003; 170:341–348. [PubMed: 12496418]
37. Popielarski SR, Pun SH, Davis ME. A nanoparticle-based model delivery system to guide the rational design of gene delivery to the liver. 1. Synthesis and characterization. Bioconjug Chem. 2005; 16:1063–1070. [PubMed: 16173781]
38. Brown SA, Hanscom HN, Vu H, Brew SA, Winkles JA. TWEAK binding to the Fn14 cysteine-rich domain depends on charged residues located in both the A1 and D2 modules. Biochem J. 2006; 397:297–304. [PubMed: 16526941]
39. Medberry CJ, Crapo PM, Siu BF, Carruthers CA, Wolf MT, Nagarkar SP, et al. Hydrogels derived from central nervous system extracellular matrix. Biomaterials. 2013; 34:1033–1040. [PubMed: 23158935]
40. Gurunathan S, Winkles JA, Ghosh S, Hayden MS. Regulation of fibroblast growth factor-inducible 14 (Fn14) expression levels via ligand-independent lysosomal degradation. J Biol Chem. 2014; 289:12976–12988. [PubMed: 24652288]
41. Schuster BS, Kim AJ, Kays JC, Kanzawa MM, Guggino WB, Boyle MP, et al. Overcoming the Cystic Fibrosis Sputum Barrier to Leading Adeno-associated Virus Gene Therapy Vectors. Mol Ther. 2014; 22:1484–1493. [PubMed: 24869933]
42. Dhruv H, Loftus JC, Narang P, Petit JL, Fameree M, Burton J, et al. Structural basis and targeting of the interaction between fibroblast growth factor-inducible 14 and tumor necrosis factor-like weak inducer of apoptosis. J Biol Chem. 2013; 288:32261–32276. [PubMed: 24056367]
43. Zhou H, Ekmekcioglu S, Marks JW, Mohamedali KA, Asrani K, Phillips KK, et al. The TWEAK receptor Fn14 is a therapeutic target in melanoma: immunotoxins targeting Fn14 receptor for malignant melanoma treatment. J Invest Dermatol. 2013; 133:1052–1062. [PubMed: 23190886]
44. Zhou H, Marks JW, Hittelman WN, Yagita H, Cheung LH, Rosenblum MG, et al. Development and characterization of a potent immunoconjugate targeting the Fn14 receptor on solid tumor cells. Mol Cancer Ther. 2011; 10:1276–1288. [PubMed: 21586630]
45. Zhou H, Hittelman WN, Yagita H, Cheung LH, Martin SS, Winkles JA, et al. Antitumor activity of a humanized, bivalent immunotoxin targeting fn14-positive solid tumors. Cancer Res. 2013; 73:4439–4450. [PubMed: 23722548]
46. Tobias A, Ahmed A, Moon KS, Lesniak MS. The art of gene therapy for glioma: a review of the challenging road to the bedside. J Neurol Neurosurg Psychiatry. 2013; 84:213–222. [PubMed: 22993449]
47. Voges J, Weber F, Reszka R, Sturm V, Jacobs A, Heiss WD, et al. Clinical protocol. Liposomal gene therapy with the herpes simplex thymidine kinase gene/ganciclovir system for the treatment of glioblastoma multiforme. Hum Gene Ther. 2002; 13:675–685. [PubMed: 11916490]
48. Voges J, Reszka R, Gossmann A, Dittmar C, Richter R, Garlip G, et al. Imaging-guided convection-enhanced delivery and gene therapy of glioblastoma. Ann Neurol. 2003; 54:479–487. [PubMed: 14520660]
49. Veiseh O, Sun C, Fang C, Bhattarai N, Gunn J, Kievit F, et al. Specific targeting of brain tumors with an optical/magnetic resonance imaging nanoprobe across the blood-brain barrier. Cancer Res. 2009; 69:6200–6207. [PubMed: 19638572]

50. Zimmermann DR, Dours-Zimmermann MT. Extracellular matrix of the central nervous system: from neglect to challenge. Histochem Cell Biol. 2008; 130:635–653. [PubMed: 18696101]

51. Willis AL, Tran NL, Chatigny JM, Charlton N, Vu H, Brown SA, et al. The fibroblast growth factor-inducible 14 receptor is highly expressed in HER2-positive breast tumors and regulates breast cancer cell invasive capacity. Mol Cancer Res. 2008; 6:725–734. [PubMed: 18505918]

52. Yin J, Liu YN, Tillman H, Barrett B, Hewitt S, Ylaya K, et al. AR-Regulated TWEAK-FN14 Pathway Promotes Prostate Cancer Bone Metastasis. Cancer Res. 2014; 74:4306–4317. [PubMed: 24970477]

53. Whitsett TG, Cheng E, Inge L, Asrani K, Jameson NM, Hostetter G, et al. Elevated expression of Fn14 in non-small cell lung cancer correlates with activated EGFR and promotes tumor cell migration and invasion. Am J Pathol. 2012; 181:111–120. [PubMed: 22634180]

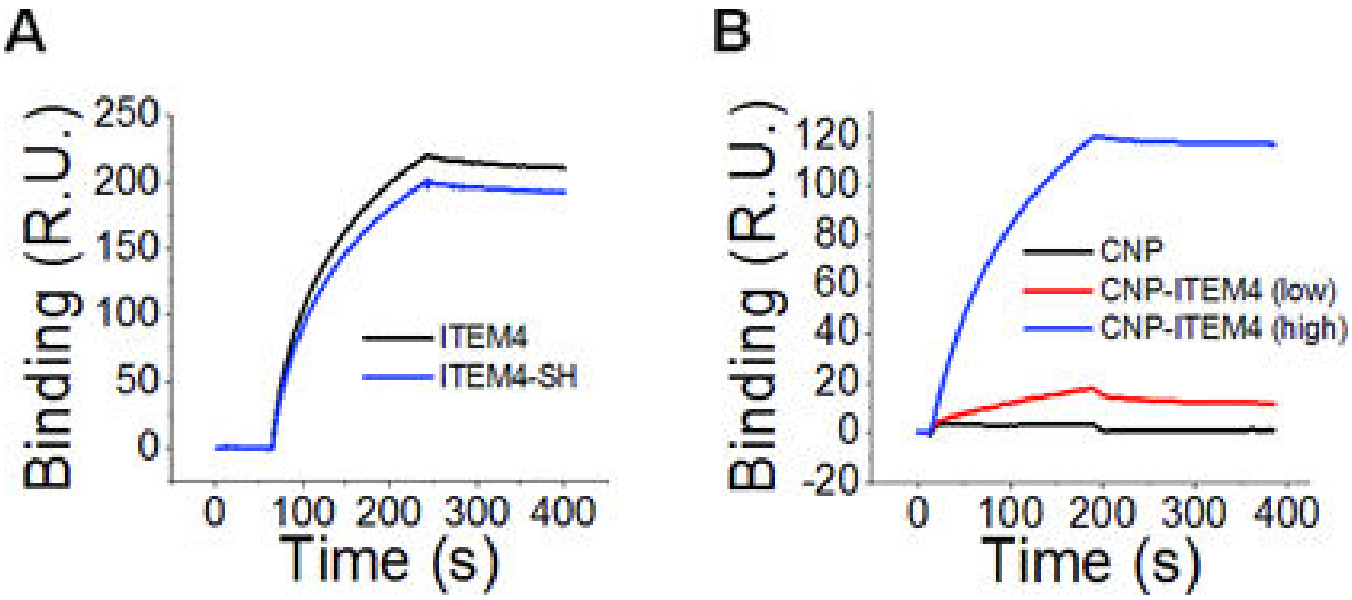

Figure 1.

Surface plasmon resonance analysis measuring antibody and nanoparticle binding to the Fn14 extracellular domain: (A) free ITEM4 and thiol-modified ITEM4 (ITEM4-SH) and (B) CNP and CNP-ITEM4 nanoparticles with two different surface densities of ITEM4.

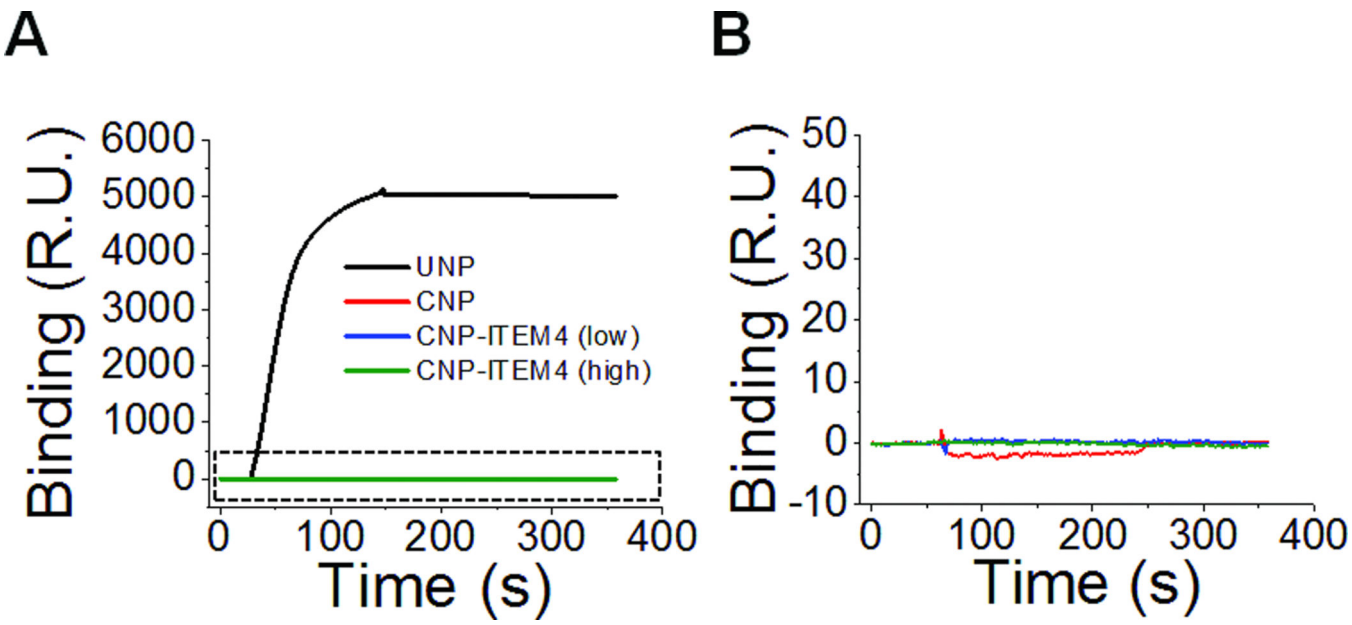

Figure 2.

Surface plasmon resonance analysis measuring the binding of (A) uncoated nanoparticles (UNP), CNP, CNP-ITEM4 (low), and CNP-ITEM4 (high) to mouse brain ECM chip. (B) Expanded view of boxed region in A.

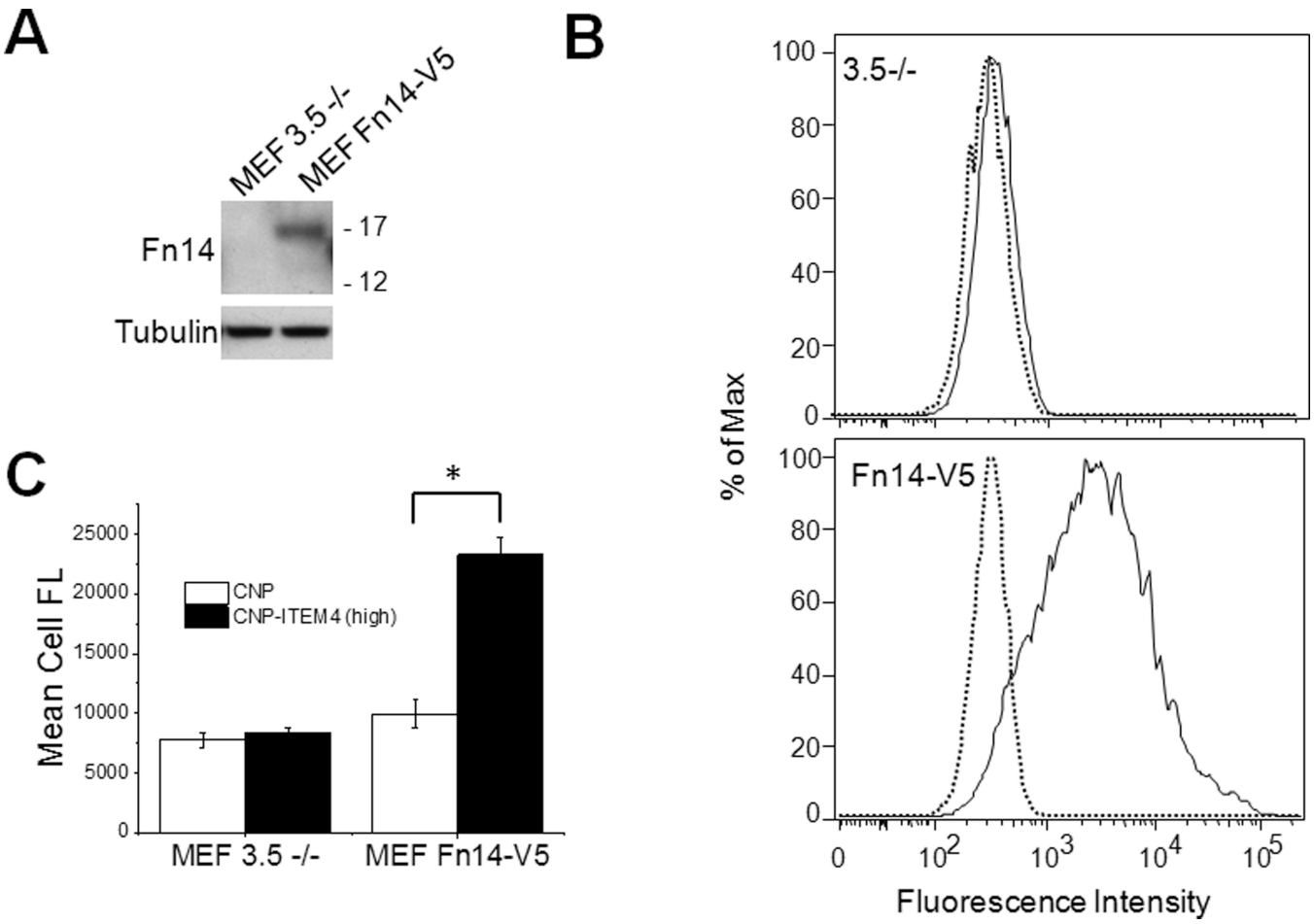

Figure 3.

Analysis of nanoparticle uptake in Fn14-positive and Fn14-negative MEFs. (A) MEF 3.5 −/− and MEF Fn14-V5 cells were harvested and Fn14 and tubulin levels were analyzed by Western blotting. (B) Flow cytometry analysis of MEF 3.5 −/− and MEF Fn14-V5 cells for Fn14 surface expression. Dotted line, mouse IgG control; solid line, ITEM4 antibody. (C) Flow cytometry analysis of CNP and CNP-ITEM4 nanoparticle uptake in MEF 3.5 −/− and MEF Fn14-V5 cells. The values shown are mean +/− SD (n=3). Data analyzed for significance using Student's t-test. *P < 0.05.

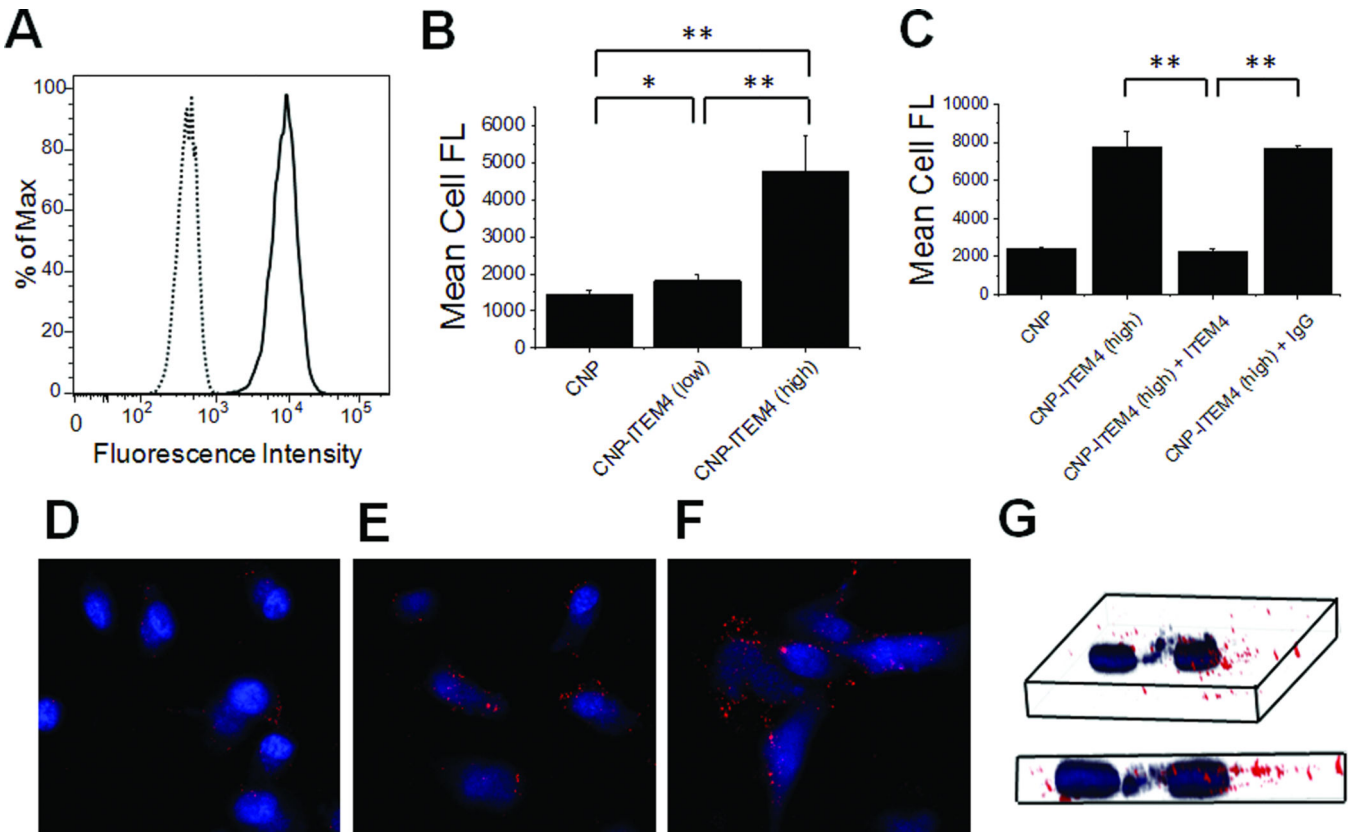

Figure 4.

Analysis of nanoparticle uptake in Fn14-positive U87 GBM cells. (A) Flow cytometry analysis of human U87 cells for Fn14 surface expression. Dotted line, mouse IgG control; solid line, ITEM4 antibody. (B) Flow cytometry analysis of CNP, CNP-ITEM4 (low), and CNP-ITEM4 (high) nanoparticle uptake in U87 cells. (C) Inhibition of nanoparticle uptake with preincubation of excess free ITEM4. In B and C, the values shown are mean +/− SD (n=3). Data analyzed for significance using Student's t-test. *P < 0.05; **P < 0.01. Confocal microscopy images of U87 cells showing association of (D) CNP, (E) CNP-ITEM4 (low), and (F) CNP-ITEM4 (high). (G) Representative 3-D projection of series of images from z-stack scan, confirming that particles (red) are inside the cell. The nucleus is stained with Hoechst 34580 (blue).

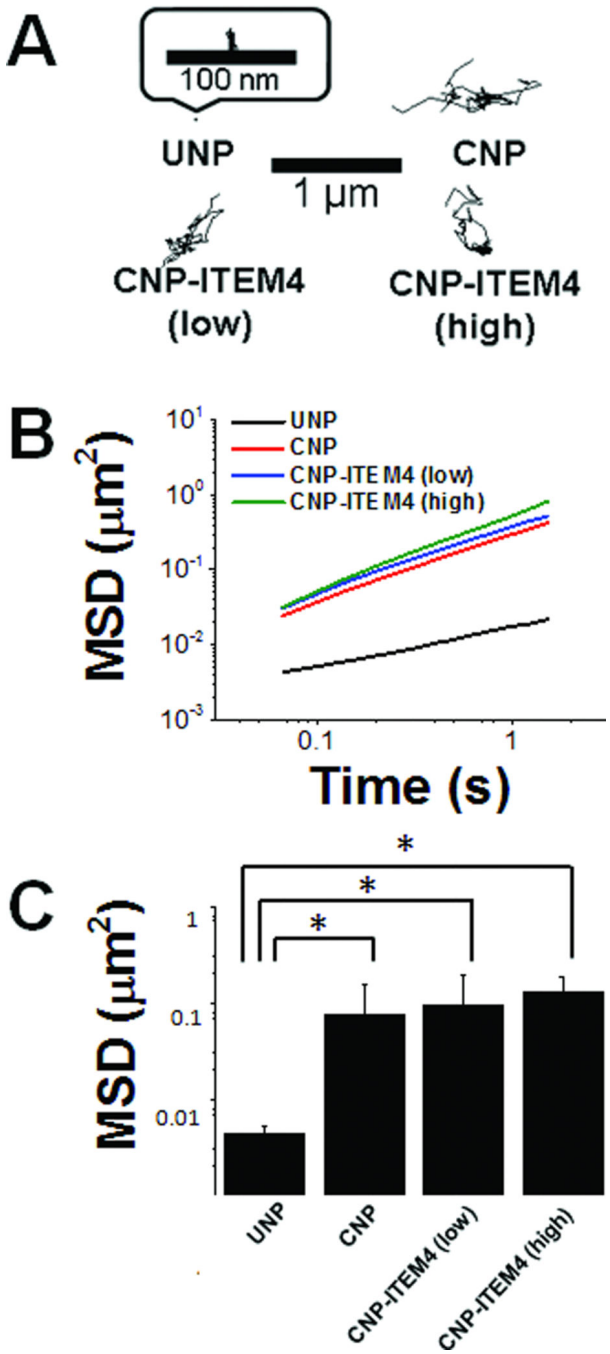

Figure 5.

Transport of nanoparticles in rat brain slices. Using MPT analysis, PEG-coated CNP-ITEM4 nanoparticles with three different surface densities of ITEM4 show enhanced transport rates compared to uncoated nanoparticles (UNP). (A) Individual particle trajectories (6 s) in rat brain slices. (B) Ensemble-averaged mean square displacements (<MSD>) as a function of time scale. (C) The ensemble-averaged MSD (<MSD>) of nanoparticles at a time scale of 1 s. Larger <MSD> values indicate faster transport rates of nanoparticles. Data represents the

average of 3 independent experiments, with n > 100 particles for each experiment. Data analyzed for significance using Student's t-test. *P < 0.05.

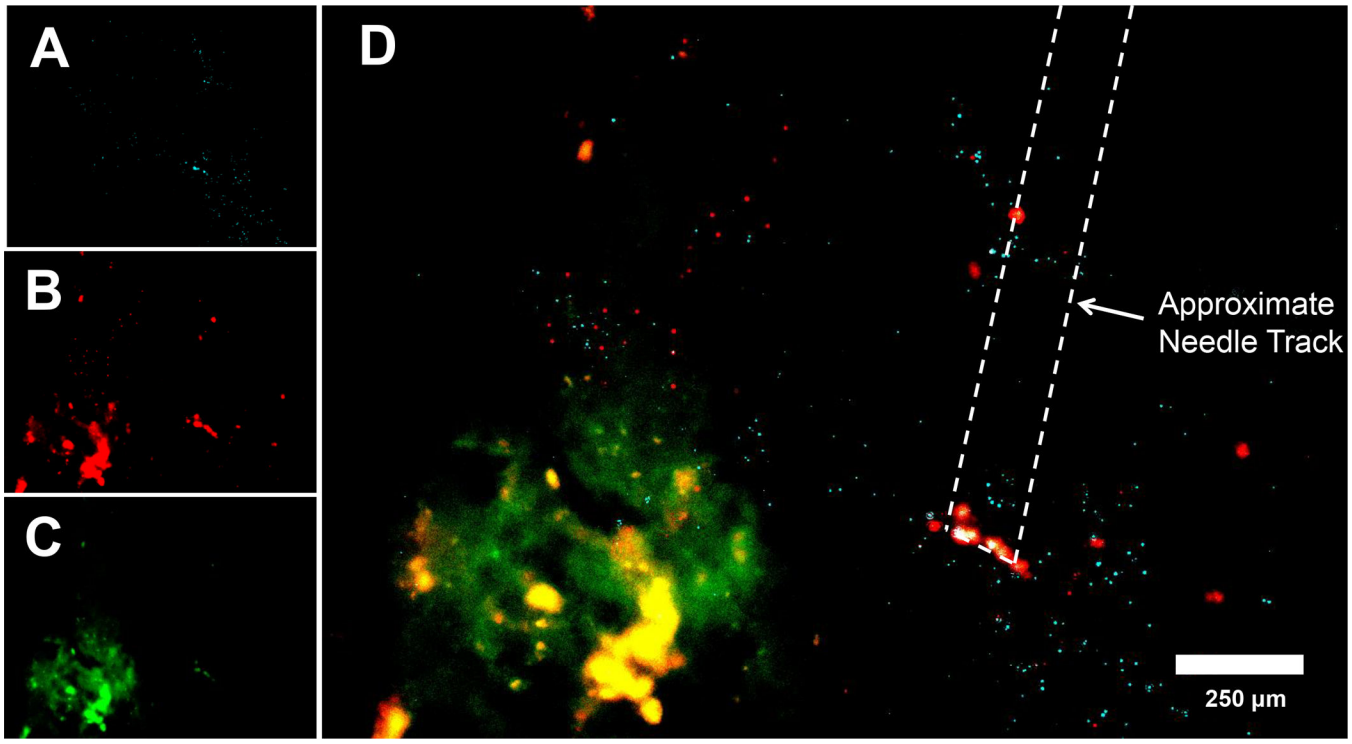

Figure 6.

In vivo distribution of nanoparticles 24 h following intracranial injection at the similar stereotactic coordinates as the U87-Luc/GFP cell tumor implantation. Representative distribution of (A) untargeted CNP nanoparticles (light blue), (B) CNP-ITEM4 (high) nanoparticles (red), and (C) GFP-expressing U87 tumors (green) in mouse striatum using fluorescence microscopy. (D) Merged image where colocalization between CNP-ITEM4 (high) and GFP-expressing U87 tumor cells is shown in yellow.

Table 1

Physicochemical properties of nanoparticles.

Formulation	Particle Diameter, (nm)[a]	ζ-potential (mV)[b]	Surface density of ITEM4 (#/particle) [c]
UNP	95 ± 3	−54.6 ± 3.0	---
CNP	113 ± 2	−7.0 ± 0.2	---
CNP-ITEM4 (low)	113 ± 3	−8.7 ± 1.2	~11
CNP-ITEM4 (high)	114 ± 22	−8.9 ± 0.7	~56

[a] Diameter (number mean) measured by dynamic light scattering. Data represents the average of 3 independent experiments +/− SD.

[b] Measured at 25°C in 15X diluted PBS, pH 7.4. Data represents the average of 3 independent experiments +/− SD.

[c] Surface density reported from LavaPep fluorescent protein assay.

Table 2

Binding affinities (K_D) of nanoparticles to the Fn14 extracellular domain.

Analyte	K_D, (nM)[a]
ITEM4	1.62
ITEM4-SH	1.57
CNP-ITEM4 (low)	0.106
CNP-ITEM4 (high)	0.024

[a] K_D values determined on a per nanoparticle basis from fit of Biacore data.